Heterogeneous bubble nucleation by homogeneous crystal nuclei in poly(L-lactic acid) foaming

Alessandra Longo[1,2,3], Ernesto Di Maio[2,3]*, Maria Laura Di Lorenzo[1]*

[1] National Research Council (CNR), Institute of Polymers, Composites and Biomaterials (IPCB), c/o Comprensorio Olivetti, Via Campi Flegrei 34, 80078 Pozzuoli, Italy

[2] Dipartimento di Ingegneria Chimica, dei Materiali e della Produzione Industriale, University of Naples Federico II, P.le Tecchio 80, Naples 80125, Italy

[3] foamlab, University of Naples Federico II, P.le Tecchio 80, Naples 80125, Italy

Abstract

A novel method to enhance and control bubble nucleation in poly(L-lactic acid) (PLLA) foaming, not relying on external nucleating agents, is presented. Amorphous PLLA was annealed at temperatures close to its glass transition, to allow local alignment of polymer chains in the form of nanosized aggregates, called homogeneous crystal nuclei (HCN). PLLA containing HCN was then foamed after sorption of CO_2 at 120°C and 10 MPa. Under the chosen experimental conditions, HCN can promote growth of PLLA spherulites that can be controlled by thermal-pressure history. Foam morphology is strongly affected by the presence of HCN, which act as heterogeneous nucleation sites for bubbles. Resulting foams were characterized by a bimodal morphology, with bubbles of about 50-70 μm in diameter developed in the bulk, and much smaller cells of few μm, grown upon pre-existing crystal aggregates. The method detailed in this manuscript to attain PLLA foams with tailored morphology can be exploited also for other semi-crystalline polymers.

Keywords: heterogeneous nucleation, PLLA, CO_2, homogeneous crystal nuclei

*Corresponding authors: edimaio@unina.it, dilorenzo@ipcb.cnr.it

Introduction

Production of plastics is increasing day by day [1] and recently the theme of plastic pollution is attracting a great research interest. Bio-based plastics are becoming increasingly important in industry as environmentally benign substitutes of plastics derived from fossil resources [2].

Poly (L-lactic acid) (PLLA) is an environmental friendly thermoplastic polyester [3]. It is bio-based and its production from biomasses releases a lower amount of carbon dioxide with respect to the production of oil-based plastics [4]. PLLA can biodegrade in nature to carbon dioxide, water, and humus-like matter [5–7] and in the human body to the natural metabolite L-lactic acid, thanks to the ester groups in its chain that make the polymer susceptible to enzymatic attack [8]. Being also biocompatible, PLLA finds applications in tissue engineering and biomedicine as medical implants [9]. Besides medical applications, PLLA is used in a variety of industrial fields, which mainly include food packaging [10], agriculture, thermal and sound insulation in construction [11], reflectors in LED lamps [12], 3D printing, in bulk or foamed form [2]. In particular, PLLA foam use is expected to grow in the near future, as promising substitute to oil-based plastics foams (e.g., polystyrene foams) [13][14]. PLLA foams are most commonly produced using CO_2 as a physical blowing agent [9,15] with a wide range of applications related to their versatility in terms of foam densities and cell morphologies, and the corresponding vast scenario of structural and functional properties has been well documented in the scientific and technical literature [13,15–18].

Designing cell morphology of the foams in terms of cell number density, dimension and other features like open/closed character, wall/strut ratio and anisotropy, has been proven effective in tuning both the functional and structural properties. Numerous strategies are available to control the processes of nucleation, growth and stabilization of foam bubbles that lead to the final cell morphology. In particular, the initial formation of bubbles, i.e bubble nucleation process, can be enhanced by the use of interfaces which ease their formation by reducing the nucleation energy barrier, as described in the context of classical (heterogeneous) nucleation theory [19,20].

Polymer compounding of PLLA with different natural and synthetic additives [21–23] and blending with other polymers have been reported as effective ways to exploit the heterogeneous bubble nucleation mechanism [15]. Presence of additives facilitates the heterogeneous nucleation at interfaces, where phase boundaries can act as nucleation sites for bubbles [24]. Incorporation of nucleating agents such as halloysite [25], microfibrillated cellulose [26], talc [27], modified silica nanoparticles [28], or hydroxyl functionalized graphene [29], have been proven effective on foaming, by reducing cells average diameter and enhancing cell number density. Unfortunately, the addition of fillers or other components to PLLA also alters the purity of the polymer, making recycling and biodegradation of the material more difficult, and may also influence its biocompatibility.

External additives (of different nature) are not the only entities which may act as heterogeneous nucleation sites. In fact, in semi-crystalline polymers, the interface between crystal and amorphous phase (of the same, neat polymer) has been proved effective as nucleating agent [15]. Numerous experimental papers addressed this issue and quantitative data correlate the number and size of cells with spherulite density and surface area [30,31] along with the modeling papers interpreting the role of the crystal/amorphous interphase. Despite the promotion of bubble nucleation, the presence of crystals along all the foaming stages may also be detrimental, sometimes preventing a fine tuning of the foam structure. In fact, crystal formation not only enhances bubble nucleation, but leads also to a decrease of the average CO_2 amount in the system, as CO_2 can be dissolved only in the amorphous areas. This in turn leads to a reduction of the fraction of sample that can undergo bubble formation, thus limiting expansion [32]. Furthermore, crystals act as physical crosslinks among the macromolecules, soon (i.e. at few percent crystalline fraction) inducing a viscosity increase which is unsuitable for the bubble growth. In other words, despite the favorable effect on bubble nucleation, crystal formation on foaming is mostly avoided, also considering the difficulty in controlling the crystalline fraction that may evolve rapidly at foaming processing conditions. In this context, it is worth of note the important effect of strain and of its rate on the crystallization, which is known as flow-induced crystallization (FIC). FIC is particularly effective in extensional (rather than shear) deformation regimes, which are in fact the ones exerted by the polymer between two growing bubbles. As a semi-crystalline polymer, foaming of PLLA requires a careful selection of processing variables, to cope with the negligible blowing agent solubility in the crystal phase, the divergent viscosity of the system during crystallization, and the interaction and mutual nucleating effect of crystals and bubbles [30,33,34], not an easy, reproducible and industrially scalable task.

Despite the above difficulties in foaming semi-crystalline polymers, in this manuscript we propose a novel procedure to exploit some features of polymer crystallization that may allow attaining foams with tailored morphology, avoiding at the same time, sizable crystal formation before foaming. Similar to foaming, polymer crystallization proceeds via crystal nucleation and growth [35,36]. Nucleation can be heterogeneous, when crystals grow upon external surfaces, cavities, or cracks of insoluble particles, or homogeneous, when few parallel polymer chain segments, called homogeneous crystal nuclei (HCN) aggregate and reach a supercritical size that is sufficiently stable to initiate crystal growth on their surface [35,36]. Compared to heterogeneous nucleation, the density of HCN is about 10^9 times larger [37], and crystals grown from HCN may be so small to grow not to the typical lamellar/spherulitic shape, but to a nodular morphology of nanometer size [38].

One important feature of homogeneous crystal nucleation is that HCN can grow to supercritical size at temperatures where crystal growth rate is negligible [39], which implies that a

proper choice of experimental conditions can allow to develop structures that can favor bubbles growth, without measurable formation of crystals [40].

The kinetics of formation of HCN has been recently investigated for PLLA, and detailed knowledge of the effect of molar mass, chain structure on their development kinetics and thermal stability is now available [41–44][45]. Based on these literature information, we have explored the feasibility of HCN as nucleation sites for bubble growth in PLLA foams, with preliminary results detailed in this manuscript. Since HCN may promote growth of both crystals and bubbles, and since CO_2 largely enhances crystal growth rate, care must be taken to tailor processing conditions, in order to limit crystal growth before expansion, as discussed below. PLLA was chosen to test this novel foaming route, but the present approach may be applied also to other foamable semi-crystalline polymers.

Experimental Section

Materials

A commercial PLLA grade with L-isomer content of 96% and melt-flow index of 6 g · (10 min)$^{-1}$ (210°C/2.16 kg), grade name PLA Lx175 [46] was kindly provided by Total Corbion (The Netherlands). Before processing, PLLA was dried in an oven at 60°C under vacuum overnight. To have a uniform sample size, PLLA pellets were compression molded with a Carver Laboratory Press at a temperature of 190°C for 2 min, without any applied pressure, to allow complete melting. After this period, a pressure of about 20 bar was applied for 2 min. Successively, the press plates equipped with cooling coils were cooled to room temperature. Slabs with thickness of 0.5 mm were obtained, which were then cut into disks of a diameter of 5 mm with a hollow punch.

Sample Preparation

A Perkin-Elmer Pyris Diamond DSC, equipped with an Intracooler II cooling system that allows cooling rates high enough to attain a fully amorphous PLLA and ensures an optimal temperature control and the reproducibility of the nucleation process was used to prepare samples with different HCN density, as well as for the subsequent crystal growth.

The instrument was calibrated in temperature and energy with a high purity indium standard, dry nitrogen at a rate of 30 ml·min^{-1} was used as purge gas.

Samples were melted at 200°C for 3 minutes, followed by rapid cooling to 0°C at a rate of 100 K·min^{-1} to attain amorphous PLLA. Literature data indicate that cooling at this rate to below T_g can prevent nuclei formation in a PLLA grade of M_w = 120 kDa and containing 4 % D-isomer [43].

Based on the procedure reported in Ref. [41], after cooling to 0°C, the samples were heated to 60°C at a rate of 100 K·min^{-1} and annealed for various nucleation times, t_n = 0.5, 2 and 4 hours.

Thermal analysis

The power-compensated DSC, described above, were used for thermal analysis of foamed and un-foamed samples.

The efficiency of nuclei formation was evaluated using Tammann's two stage crystal nuclei development method, which consists in evaluating HCN formation after their growth to crystals at higher temperature [47,48]. Specifically, after nucleation at 60°C for various t_n, the samples were heated at 100 K·min^{-1} to 120°C and allowed to crystallize at 120°C for 3 min, then rapidly cooled to 0°C at a rate of 100 K·min^{-1} to prevent additional formation of crystals.

Thermal properties of the samples, before and after foaming, were analyzed upon heating at 20 K·min^{-1}. To gain precise heat capacity data from the heat flow rate measurements, each scan was accompanied by a reference empty pan run. Each measurement was repeated three times to ensure reproducibility.

Preparation of PLLA foams

Foaming was conducted in a batch autoclave named “minibatch” extensively described in [49] using CO_2 as blowing agent (SOL Group, Italy). The autoclave consists in a chamber with approximate volume of 1 cm^3, equipped with a Pt100 temperature sensor (TR1M, GEFRAN) to control the temperature by a PID controller (Ascon. New England temperature solutions, Attleboro, MA, X1), a gas dosing port connected to a syringe pump 500D (Teledyne Isco, Lincoln, NE) and a pressure transducer (F031047, GEFRAN) used to measure the pressure. The pressure release system consists of a pneumatic electrovalve (TSR-20, TruTorq Actuators), designed to ensure a fast depressurization rate of the order of 10 MPa·s^{-1}. Samples were charged by a port equipped with a quick connection to allow fast sample removal operations.

Autoclave temperature was set to 120°C and the sample was placed in the chamber after pre-set temperature was reached, to limit crystallization before foaming. CO_2 was injected into the autoclave to reach a pressure of 10 MPa. Samples were saturated for 3 minutes, then the pressure was released to atmospheric pressure (0.1 MPa) at a rate of 50 MPa·s^{-1} to obtain foamed samples. Considering the available diffusivity data of PLLA/CO_2 system [15], 3 minutes can be considered sufficient to attain a uniform CO_2 concentration within the 0.5 mm thick slab, since the characteristic diffusion time (τ_D) is:

$$\tau_D = \frac{(0.5/2\ mm)^2}{D_{CO_2-PLLA}} \sim 10^2 s \quad (1)$$

where $D_{CO_2-PLLA} = 6 \cdot 10^{-3}\ mm^2 \cdot s^{-1}$.

The thermal and pressure protocol used for PLLA foaming is sketched in Figure 1. Sample codes are reported in Table 1, where samples analyzed before foaming are identified by a "B" and the foamed formulations are identified by an "F", and followed by number referring to t_n.

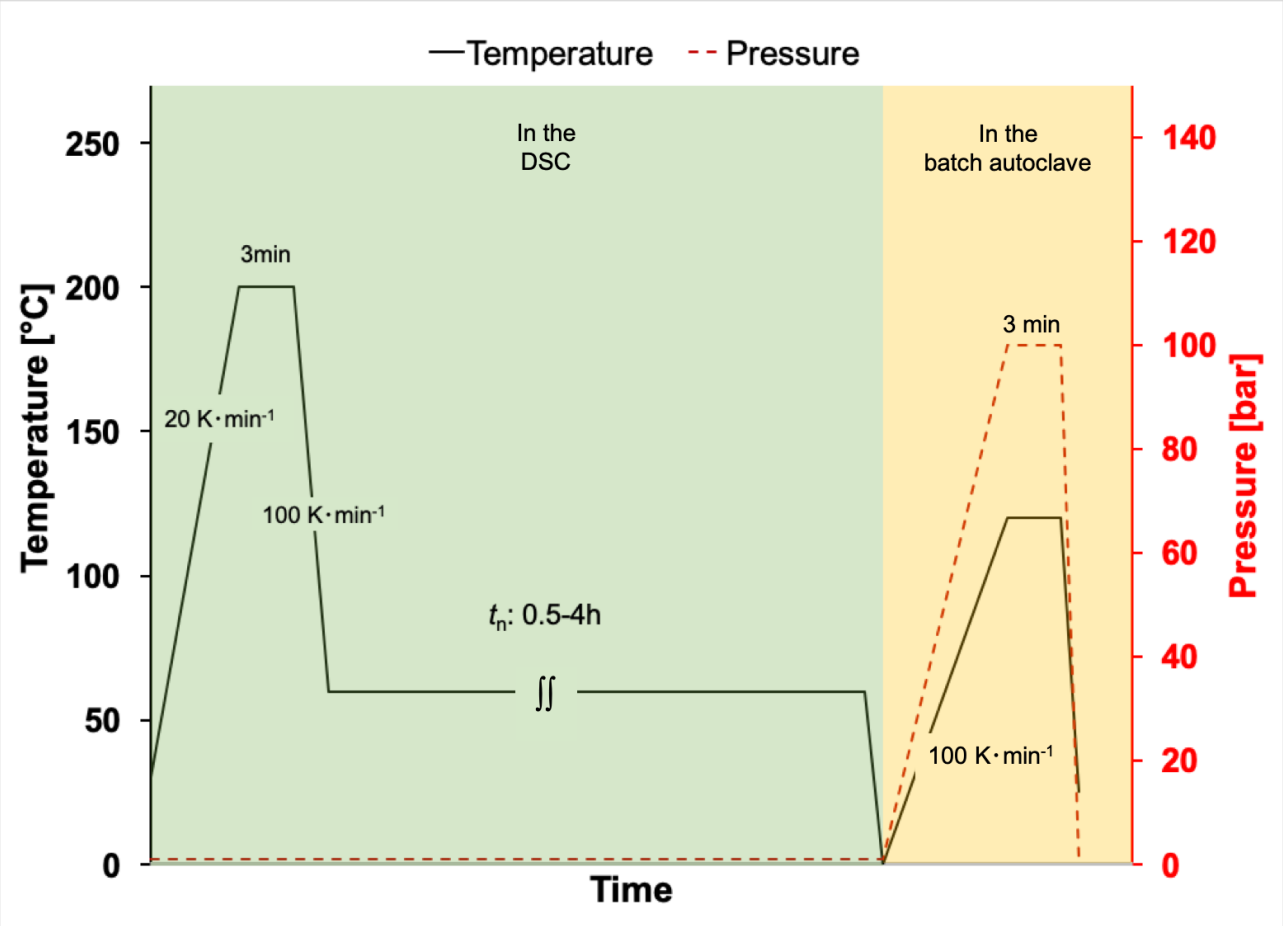

Figure 1. Scheme of the employed thermal and pressure protocol for PLLA foaming.

Table 1. Sample codes

Sample	t_n (h)	Foaming
B-0	0	No
B-0.5	0.5	No
B-2	2	No
B-4	4	No
F-0	0	Yes
F-0.5	0.5	Yes
F-2	2	Yes
F-4	4	Yes

Scanning electron microscopy

Foam morphology was evaluated using a FEI Quanta 200 FEG Scanning Electron Microscope. Before analysis the foams were blade cut and double sputtered/coated with an Au-Pd alloy using a Baltech Med 020 Sputter Coater System, then mounted on aluminum stubs.

The number density of nucleated cells, N_0, was calculated by [50]:

$$N_0 = \left({}^{n}/_{A}\right)^{3/2} \varphi \tag{2}$$

where n is the number of cells counted in A, the area of micrograph and φ is expansion ratio calculated as:

$$\varphi = \frac{\rho_{Bulk}}{\rho_{Foam}} \tag{3}$$

where ρ_{Bulk} and ρ_{Foam} are bulk densities of neat PLLA and of foamed sample (in g·cm^{-3}) respectively measured according to ASTM-D1622-03.

X-ray Diffraction (XRD)

X-ray diffraction spectra were collected with a PANalytical X'PertPro diffractometer equipped with a PIXCel 1D detector, under CuKα radiation. Sample spectra were collected in the range 5-40° 2θ, with a step size of 0.013° 2θ and counting time of 20 s per step.

Optical Microscopy

A Zeiss Axioskop Polarized Optical Microscope (POM) equipped with a Linkam THMS 600 hot stage and a Scion Corporation CFW-1312C Digital Camera was used to quantify crystal nucleation.

Images were captured with Image-Pro Plus 7.0 software (Media Cybernetics). A thin film of PLLA was obtained by squeezing samples between two glass slips on a hot plate, and then thermal treated using the same thermal protocol detailed before: amorphous PLLA was annealed at 60°C for various t_n, then heated to 120°C for 3 min in a hot stage. At the end of the crystallization step, samples were quenched in liquid nitrogen to stop further crystal growth. Nitrogen gas was fluxed in the hot stage during thermal treatment to prevent degradation. The optical micrographs were used to evaluate the spherulite number density (S_0) per unit area, evaluated upon an area of ~ $1 \cdot 10^{-3}$ cm^2.

Results and discussion

Literature data on nucleation kinetics of PLLA indicate that, for a grade with melt flow index 6 g · (10 min)$^{-1}$ (210°C/2.16 kg) and containing 4 % of D-isomer, i.e. with similar molar mass and stereoregularity of the polymer used here, the onset time of crystal nucleation is around 0.3 h at 60°C [43]. Based on this piece of information, three different t_n were selected, from 0.5 to 4 h, and the efficiency of crystal nucleation was quantified using Tamman's method [47,48], with samples maintained at 120°C for 3 min to allow spherulite growth after HCN formation.

The apparent specific heat capacity data (c_p) of PLLA annealed at 60°C for various t_n then crystallized at 120°C is presented in Figure 2. Sample B-0, i.e. the polymer quenched from the melt to below T_g and immediately reheated to 120°C, displays a step-like increase of the heat capacity at 60°C due to glass transition and, on further heating, a small endotherm centered around 160°C revealing melting of crystals grown at 120°C. Annealing at 60°C before crystallization at 120°C leads to an increase of the area of the melting peak, which becomes more pronounced with the increase of t_n (samples B-0.5, B-2, B-4). This is due to an increased fraction of crystals grown at 120°C within the pre-defined crystallization time of 3 min, and is paralleled by a progressive decrease of the heat-capacity step at T_g, due to the lower amorphous fraction.

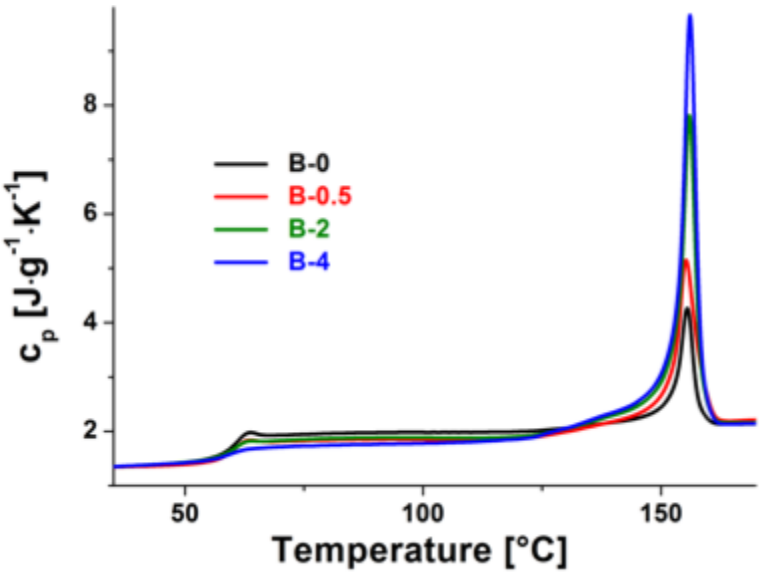

Figure 2. Apparent heat capacity (c_p) of PLLA after annealing at 60°C, followed by isothermal crystallization at 120°C, measured upon heating at 20 K·min^{-1}.

Integration of the endothermic peaks and comparison with enthalpy of melting of 100% crystalline PLLA [51] yields the crystal fraction (X_C), with data reported in Table 2. Crystallinity of PLLA sizably increases with t_n, from $X_C = 0.07$ for B-0 to $X_C = 0.28$ for B-4. These data indicate that progressive increase of t_n leads to a corresponding increase of the density of HCN, which in turn favors growth of a larger number of spherulites, and results in a higher X_C, in line with literature data [41–43,52,53].

Table 2 X_C of PLLA developed after annealing at 60°C for t_n, followed by isothermal crystallization at 120°C for 3 min.

Sample	X_C
B-0	0.07
B-0.5	0.14
B-2	0.21
B-4	0.28

The variation of the density of crystal nuclei caused by the different t_n was confirmed by polarized optical microscopy (POM). Since HCN are not visible with POM, Tamman's two-stage

nuclei method has been exploited also in this analysis. The optical micrographs shown in Figure 3, illustrate the influence of t_n on PLLA morphology.

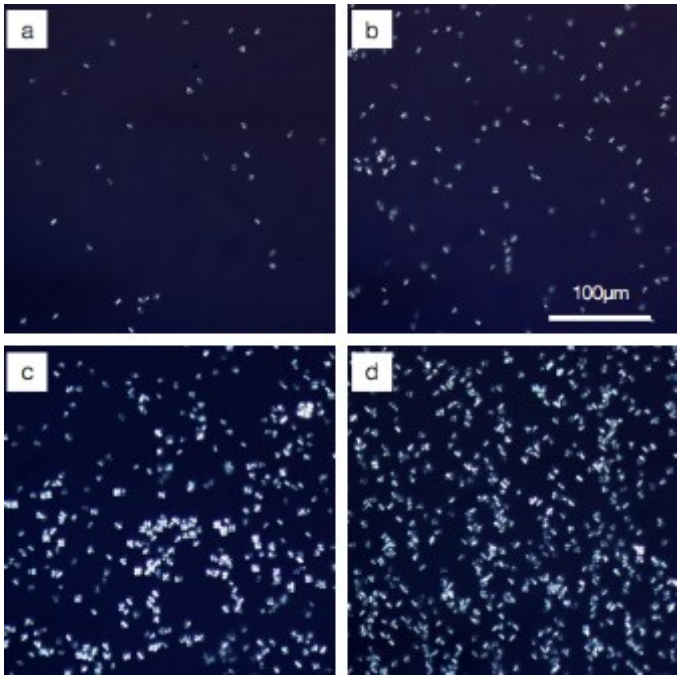

Figure 3. POM micrographs of PLLA cold crystallized at 120°C for 3 min after aging at 60°C for various t_n: a) B-0; b) B-0.5; c) B-2; d) B-4.

The optical micrographs of Figure 3 display, for all samples, PLLA spherulites with about 6.5 µm diameter developed after 3 min of isothermal crystallization at 120°C. Moreover, the spherulites number density (S_0) increases with t_n. This increase is quantified in Figure 4, which displays S_0 as function of t_n. On the same plot, the variation of X_C with t_n (data retrieved from Table 2), is also shown for comparison. S_0 progressively increases of about one order of magnitude from B-0 to B-4, and is paralleled by a corresponding increase of X_C for samples subjected to the same thermal history, which in turn is linked to the higher number of crystals growing on HCN. In other words, POM analysis, in line with DSC data, confirm that the chosen experimental conditions lead to a sizably varied number density of HCN with increasing t_n at 60°C, in agreement with literature data [36].

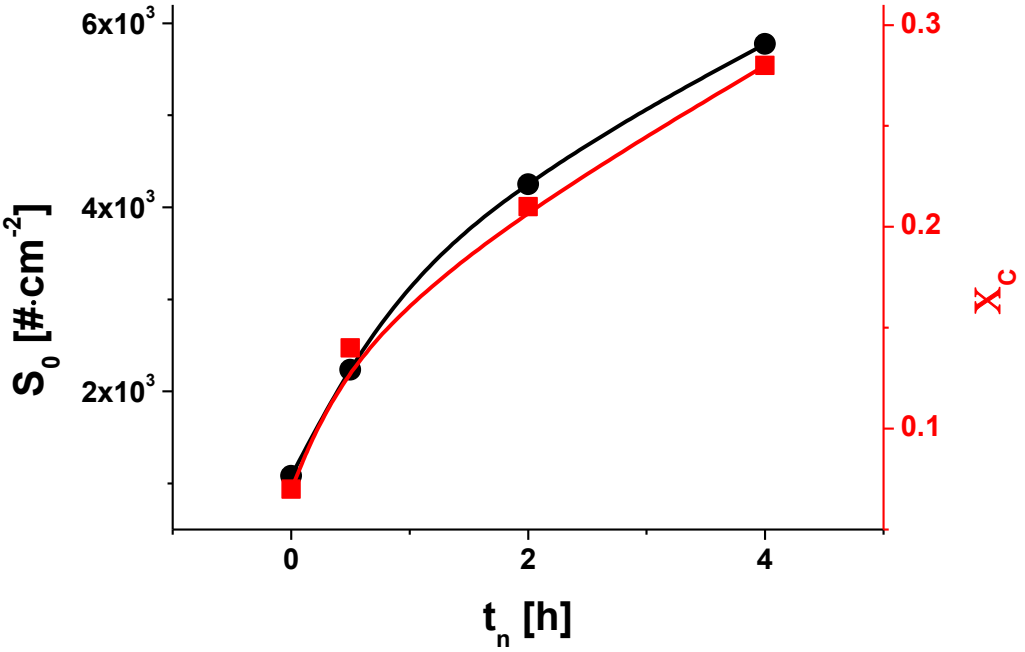

Figure 4. S_0 (black circles) as a function of t_n at 60°C, determined from optical micrographs of Figure 3, compared with X_C (red squares) measured by DSC plots of Figure 2.

In foaming experiments, PLLA samples annealed for various t_n at 60°C were utilized. In this case, the crystallization was conducted in the autoclave under CO_2 pressure at 10 MPa, 120°C for 3 minutes. The resulting foamed samples, F-0 to F-4 were analyzed in terms of cellular morphology and expansion ratio. The cellular morphology of obtained foams is illustrated in Figure 5. F-0 and F-0.5 display a uniform morphology, with only some slight reduction in bubble size of sample nucleated for 0.5 h before foaming. When PLLA is maintained for longer time at 60°C, the foam morphology becomes bimodal, with the formation of two types of cells, as seen in Figures 5-C and 5-D: large bubbles developed in the bulk, and much smaller cells grown in a "stamen-like cell structure", where round entities corresponding to PLLA spherulites appear surrounded by several elongated cells [54]. This morphology reveals heterogeneous nucleation of cells on a bubble nucleating site, which in this case is the spherulite [54]. The spherulites were grown before foaming, during the sorption step. Looking at Figure 4, which reports the optical micrographs of PLLA spherulites grown at 120°C for 3 min in N_2 at atmospheric pressure after homogeneous crystal nucleation at 60°C, a t_n = 0.5 h leads to only a minor increase of crystal nucleation density, which rationalizes the similar morphology of the foams displayed in Figures 5-a and 5-b. Conversely, a marked increase of crystal nucleation density is revealed after annealing PLLA at 60°C for longer times, $t_n \geq 2$ h: these HCN grow to small

spherulites during the 3-minute sorption of CO_2, and act as solid substrate/interface for bubble growth. The average diameter of the spherulites seen in Figure 5 is around 20 ± 10 μm, only slighter larger than the same spherulites grown at the same temperature for the same time under N_2 at atmospheric pressure (see Figure 3), whose diameter is 6.5 μm, as reported above. The somewhat higher size of the spherulites seen in Figure 5 is to be linked to the faster spherulite growth rate of PLLA in the presence of CO_2, which plasticizes the polymer, as well documented in the literature [55–57].

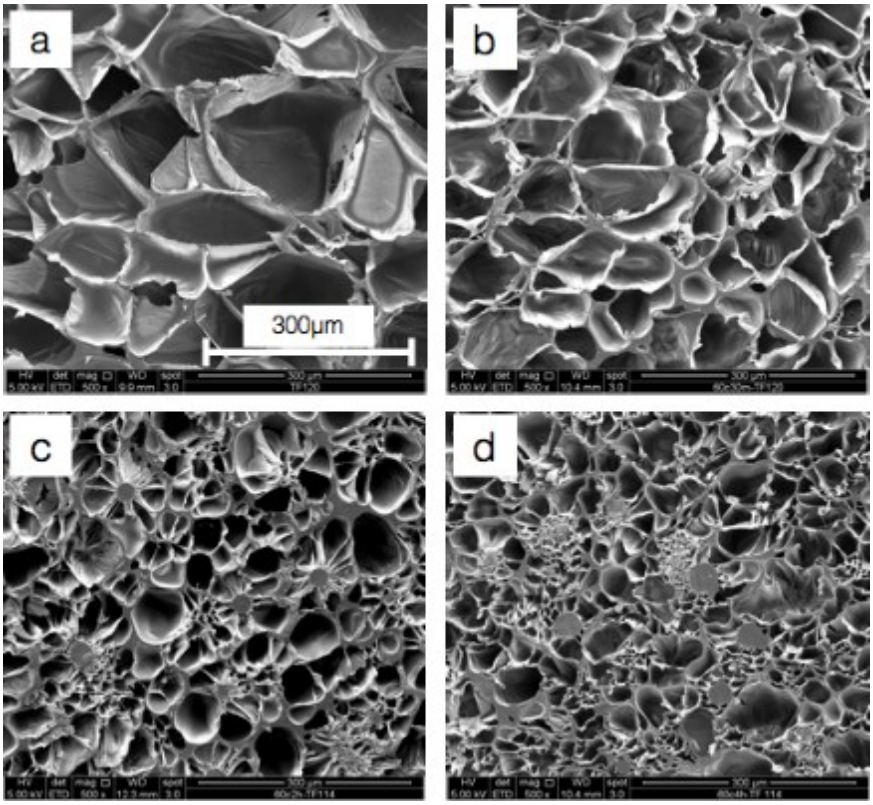

Figure 5. SEM micrographs of PLLA foamed after annealing at 60°C for t_n ranging from 0 to 4 h, followed by 3-minute sorption of CO_2 at 10 MPa and 120°C: a) F-0; b) F-0.5; c) F-2; d) F-4.

The electron micrographs of Figure 5 were used to calculate the average cell size, measured averaging the larger and smaller diameters of elongated bubble, and number density of nucleated cells, N_0, reported in Figure 6. The patterned data points reveal the overall increase of N_0 with t_n, whereas the close and open data points distinguish cells grown in the bulk and in the stamen-like regions, respectively. On the same plot, the average cell size data are also presented, again with open and close symbols for samples that display a bimodal morphology and hatched data referring to the average value. Increasing t_n leads to an overall increase of bubble number, whose average size also

progressively decreases with t_n. Sample F-4, foamed after HCN development for 4 h at 60°C, displays the largest N_0 ($1.1 \cdot 10^7$ cells·cm^{-3}) and the smallest cell size both in the bulk and in the stamen-like regions, with a decrease of bubble size of 2 orders of magnitude in the stamen-like regions, compared to F-0.

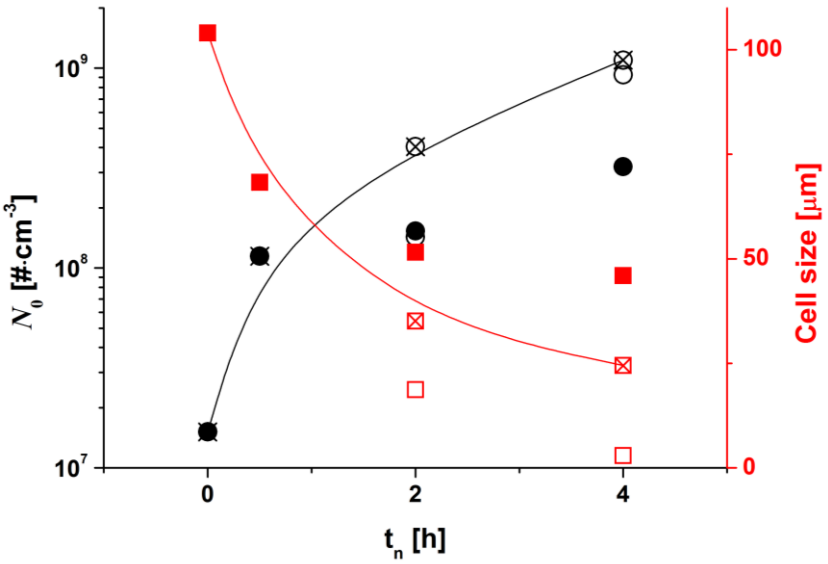

Figure 6 N_0 (black circles) and cell size (red squares) of foams as a function of t_n. The close and open symbols refer to bulk and stamen regions, respectively, the hatched data are the total N_0 and average values for cell size.

Data of expansion ratio (φ), i.e. the ratio between density of bulk and foamed PLLA (eq. 3), are presented in Table 3. A non-monotonic variation of φ is evident from the data, as sample F-0.5 displays a remarkable gain in expansion ratio compared to F-0, with φ that decreases in PLLA foamed after longer t_n.

Table 3. Expansion ratio of PLLA foams

Sample	φ
F-0	7.75
F-0.5	24.8
F-2	15.5
F-4	20.7

Additional information on the effect of annealing at 60°C before foaming is revealed by comparison of the volume fraction of the cells, estimated from SEM micrographs, with degree of expansion. Having determined N_0 both in bulk ($N_{0_{Bulk}}$) and stamen-like ($N_{0_{Stamen}}$) areas, and having measured the corresponding representative cell diameter ($Size_{Bulk}$ and $Size_{Stamen}$), it is possible to estimate the total void volume (V_V) by combining the volume of the two different type of cells (v_{Bulk} and v_{Stamen}). By normalizing V_V, one may infer about the contribution to expansion by large and small cells to justify non-monotonic effect of t_n on φ.

Partial v values of bulk (v_{Bulk}) and stamen (v_{Stamen}) cells are presented in Figure 7 as function of t_n. On the same plot, the expansion ratio data, taken from Table 3 are also shown. Both v_{Bulk} and φ display similar non-monotonic trend with t_n, with a much higher volume and larger expansion attained when PLLA is foamed after annealing at 60°C for 0.5 h. It is also clearly visible how small stamen cells contribute in a small way to V_V and therefore to expansion, possibly justifying the reduced expansion at larger t_n.

To further rationalize the large expansion and volume of sample F-0.5, crystallization kinetics of PLLA needs to be taken into account. As shown in Figures 2, annealing PLLA at 60°C for 0.5 h before crystal growth at 120°C, leads to an only minor increase in X_C, whereas sizable increase in crystallinity takes place when the polymer is annealed at 60°C for longer t_n. By recalling that the crystalline phase is impermeable to the blowing agent, in samples with low X_C only a minor reduction of CO_2 sorption takes place when the polymer is placed within the foaming reactor at 120°C under CO_2 at 10 MPa. Conversely, in samples with larger X_C, the amount of blowing agent is reduced.

It is worth to remember to the reader that data shown in Figure 2 were measured under N_2 flow at atmospheric pressure which has negligible effect on crystallization kinetics with respect to the plasticization due to CO_2 [56]. This makes the comparison between X_C gained during DSC or microscopy analysis and during the overall foaming process only qualitative.

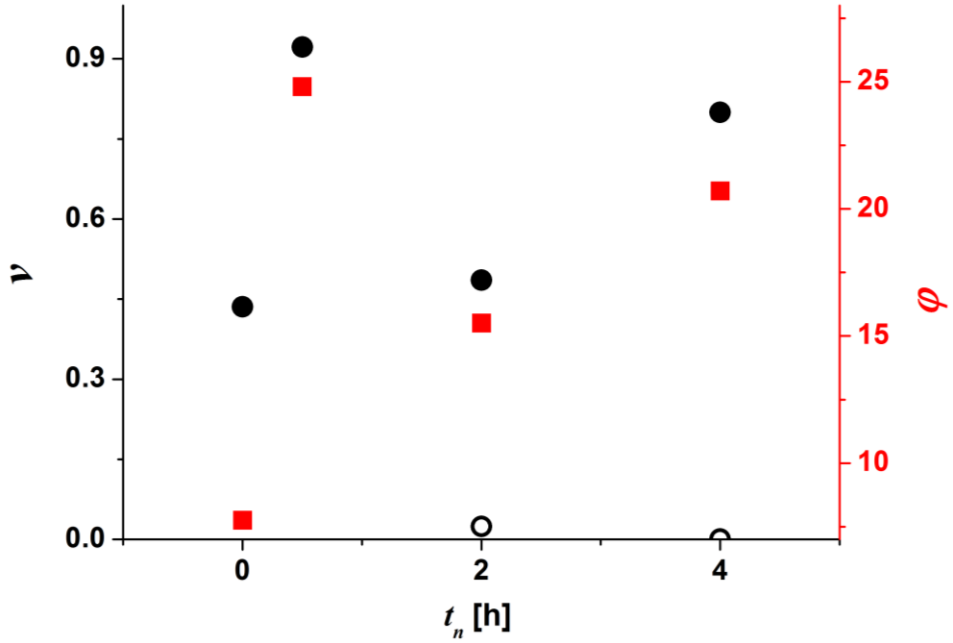

Fig 7. v_{Bulk} (filled circles), v_{Stamen} (empty circles) and φ (squares) as functions of t_n

To complete details of the feasibility of the proposed method, thermal and structural analysis of PLLA foams are presented in Figures 8 and 9. Figure 8 illustrates the heat capacity plots of PLLA foams, whose morphology is illustrated in Figure 5. The various foams display only minor differences in thermal output, all having a X_C around 0.34, slightly higher when compared with B-4 (X_C = 0.28). Despite the varied initial crystallinity before foaming, flow-induced crystallization (FIC) occurs upon bubble development, and results in a comparable development of crystal fraction in all the analyzed samples. It is worth to note that the polymer further crystallizes upon DSC heating for all samples, as revealed by the cold crystallization exotherm centered around 110°C, well visible for all samples.

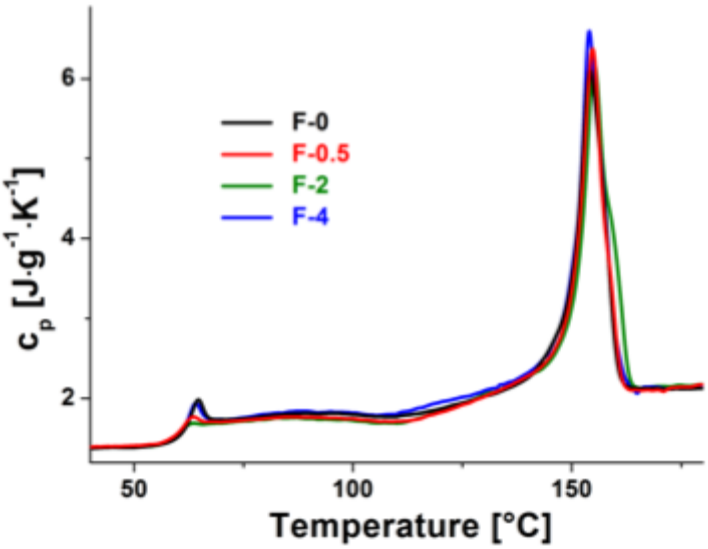

Figure 8. Apparent specific heat capacity (c_p) of PLLA foams, measured upon heating at 20 K·min^{-1}.

X-ray diffraction analysis of the foams is exampled in Figure 9 for sample F-4, being similar to X-ray diffraction patterns of the other foamed samples. The diffraction pattern shown in Figure 9 is typical of α-crystal modification of PLLA: the spectrum presents main diffraction peaks at 2θ = 16.5 and 19 °, plus a reflection at 22.2 °, which is observed only in PLLA containing α-crystals, and the reflection at 24.5 ° characteristic of α'-crystals is absent [58,59]. The X-ray profile of Figure 9 is in agreement with literature data, which indicate that foaming of semi-crystalline PLLA leads to growth of α-crystals, even in the presence of nucleating sites [60,61], proving the proposed strategy of foaming PLLA in the presence of HCN does not affect structural properties of PLLA foams.

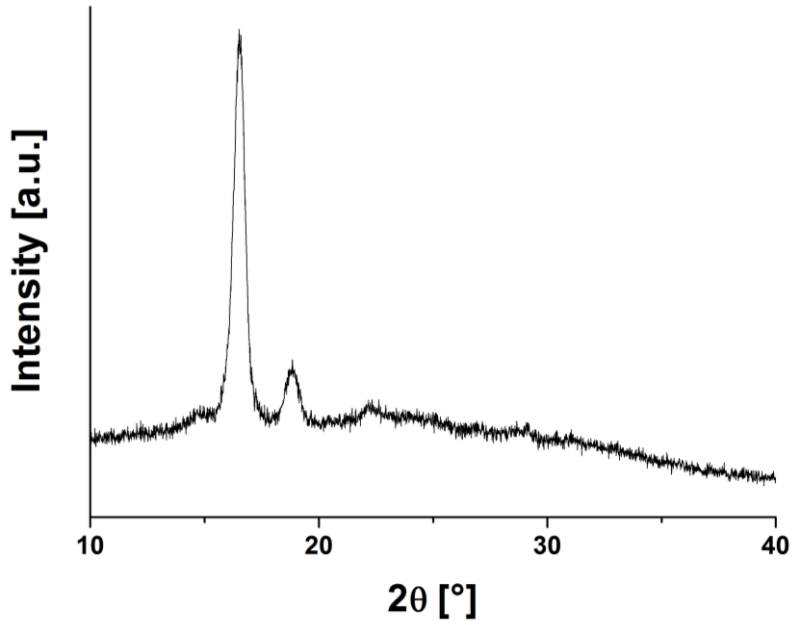

Figure 9. X-ray diffraction pattern of PLLA foamed after annealing at 60°C for t_n = 4 (sample F-4).

Conclusions

PLLA slabs with a thickness of 0.5 mm were homogeneously nucleated by annealing at T_g for a t_n varying from 0.5 to 4 h. The increase in t_n results in an increased spherulites number density S_0, grown on homogeneous nuclei. Nucleated samples were physical foamed at 120°C and 10 MPa of CO_2 with a sorption time of 3 minutes. The foams display minor differences in thermal properties, all having a X_C around 0.34 and the same α-crystals form of the neat polymer.

The morphology of the foams was observed with SEM and the increasing in t_n leads to a monotone decrease in cell size and larger bubble density. Samples with t_n 2 and 4 h, show a bi-modal morphology with the formation of two different types of cells, bigger in the bulk and smaller stamen-like cells surrounding growing crystals. The expansion ratio ranged from 7.75 to 24.8 with the maximum value for the sample nucleated for t_n = 0.5 h.

The enhancement in foam expansion ratio and morphology due to the presence of homogeneous crystal nuclei, corroborate the advantages of this method to improve foaming of PLLA, avoiding the addition of heterogeneous additives, thereby preserving its biodegradability and biocompatibility.

Acknowledgements

The authors warmly thank Ms. Maria Cristina Del Barone of IPCB-CNR and Prof. Paolo Aprea of DICMaPI-UniNa for their assistance with SEM and X-ray diffraction analyses, respectively .

Data availability

The raw/processed data required to reproduce these findings cannot be shared at this time as the data also forms part of an ongoing study

References

[1] S.B. Borrelle, J. Ringma, K. L. Law, C.C. Monnahan, L. Lebreton, A. McGivern, E. Murphy, J. Jambeck, G. H. Leonard, M. A. Hilleary, M. Eriksen, H. P. Possingham, H. De Frond, L. R. Gerber, B. Polidoro, A. Tahir, M. Bernard, N. Mallos, M. Barnes, C. M. Rochman, *Science* **2020**, *369*, 1515.

[2] B. Gupta, N. Revagade, J. Hilborn, *Prog. Polym. Sci.* **2007**, *32*, 455.

[3] M. L. Di Lorenzo, R. Androsch, *Industrial Applications of Poly(lactic acid)*, *Adv. Polym. Sci.*, Vol. 282 Springer, Cham, **2018**.

[4] R. N. Darie-Niţə, C. Vasile, A. Irimia, R. Lipşa, M. Râpə, *J. Appl. Polym. Sci.* **2016**, *133*, 43223.

[5] R. Gattin, A. Copinet, C. Bertrand, Y. Couturier, *J. Appl. Polym. Sci.* **2003**, *88*, 825.

[6] M. L. Di Lorenzo, R. Androsch, *Synthesis, Structure and Properties of Poly(lactic acid)*, *Adv. Polym. Sci.*, Vol. 279, Springer, Cham, **2018**.

[7] R. E. Drumright, P. R. Gruber, D. E. Henton, *Adv. Mater.* **2000**, *12*, 1841.

[8] D. Zhang, M. A. Kandadai, J. Cech, S. Roth, S. A. Curran, *J. Phys. Chem. B.* **2006**, *110*, 12910.

[9] P. Netti, *Biomedical foams for tissue engineering applications*, Woodhead Publishing, **2014**.

[10] L. Wang, R. E. Lee, G. Wang, R. K. M. M. Chu, J. Zhao, C. B. Park, *Chem. Eng. J.* **2017**, *327* 1151.

[11] J. M. Julien, J. C. Quantin, J.C. Bénézet, A. Bergeret, M. F. Lacrampe, P. Krawczak, *Eur. Polym. J.* **2015**, *67*, 40.

[12] C. C. Kuo, L. C. Liu, W. C. Liang, H. C. Liu, C. M. Chen, *Mater. Res. Bull.* **2015**, *67*, 170.

[13] K. Parker, J. P. Garancher, S. Shah, S. Weal, A. Fernyhough, in:*Handbook of Bioplastics and Biocomposites Engineering Applications* (Ed: S. Pilla), Scrivener Publishing, Salem, MA, 2011, Ch. 6.
[14] K. Parker, J. P. Garancher, S. Shah, A. Fernyhough, *J. Cell. Plast.* **2011**, *47*, 233.
[15] M. Nofar, C. B. Park, *Prog. Polym. Sci.* **2014**, *39*, 1721.
[16] S. G. Mosanenzadeh, H. E. Naguib, C. B. Park, N. Atalla, *Polym. Eng. Sci.* **2013**, *53*, 1979.
[17] M. Ajioka, K. Enomoto, A. Yamaguchi, K. Suzuki, T. Watanabe, Y. Kitahara (Mitsui Chemicals Inc.), US5447962A, **1995**.
[18] P. Tiwary, C. B. Park, M. Kontopoulou, *Eur. Polym. J.* **2017**, *91*, 283.
[19] S. N. Leung, A. Wong, L. C. Wang, C. B. Park, *J. Supercrit. Fluids.* **2012**, *63*, 187.
[20] C. Wang, S. N. Leung, M. Bussmann, W. T. Zhai, C. B. Park, *Ind. Eng. Chem. Res.* **2010**, *49*, 12783.
[21] M. Mihai, M. A. Huneault, B. D. Favis, H. Li, *Macromol. Biosci.* **2007**, *7*, 907–920.
[22] Y. Wu, X. Zhou, J. Li, K. Yu, L. Wang, J. Ma, *J. Phys. Chem. B.* **2021**, *125*, 6709.
[23] J. Zhang, X. Sun, *J. Appl. Polym. Sci.* **2007**, *106*, 857.
[24] J. A. Sarver, E. Kiran, *J. Supercrit. Fluids.* **2021**, *173*, 105166.
[25] B. Morlin, K. Litauszki, R. Petrény, Á. Kmetty, L. Mészáros, **2021**, *178*, 109385.
[26] C. I. R. Boissard, P. E. Bourban, C. J. G. Plummer, R. C. Neagu, J. A. E. Månson, *J. Cell. Plast.* **2012**, *48*, 445.
[27] A. Ameli, D. Jahani, M. Nofar, P. U. Jung, C.B. Park, *J. Cell. Plast.* **2013**, *49*, 351.
[28] E. J. Jeong, C. K. Park, S. H. Kim, *J. Appl. Polym. Sci.* **2020**, *137*, 48616.
[29] X. Wang, J. Mi, H. Zhou, X. Wang, *J. Mater. Sci.* **2019**, *54*, 3863.
[30] K. Taki, D. Kitano, M. Ohshima, *Ind. Eng. Chem. Res.* **2011**, *50*, 3247.
[31] Q. Ren, J. Wang, W. Zhai, S. Su, *Ind. Eng. Chem. Res.* 2013, *52*, 13411.
[32] X. Zhang, W. Ding, N. Zhao, J. Chen, C. B. Park, *Ind. Eng. Chem. Res.* **2018**, *57*, 2094.
[33] W. Zhai, Y. Ko, W. Zhu, A. Wong, C. B. Park, *Int. J. Mol. Sci.* **2009**, *10*, 5381.
[34] X. Liao, A. V. Nawaby, P.S. Whitfield, *Polym. Int.* **2010**, *59*, 1709.
[35] B. Wunderlich, *Macromolecular Physics, Vol. 2: Crystal nucleation, growth, annealing*. Academic Press, New York, **1976**.
[36] L. Mandelkern, *Crystallization of Polymers: Volume 2, Kinetics and Mechanisms*, Cambridge University Press, **2004**.
[37] R. Androsch, A. M. Rhoades, I. Stolte, C. Schick, *Eur. Polym. J.* **2015**, *66*, 180.
[38] R. Androsch, B. Wunderlich, *Polymer* **2005**, *46*, 12556.

[39] R. Androsch, M. L. Di Lorenzo, C. Schick, in *Synthesis, Structure and Properties of Poly(lactic acid)*, Vol. 279 (Eds. M. L. Di Lorenzo, R. Androsch), Springer, Cham **2018**, Ch. 7.
[40] J. W. P. Schmelzer, A. S. Abyzov, V. M. Fokin, C. Schick, E. D. Zanotto, *J. Non. Cryst. Sol.* **2015**, *429*, 24.
[41] R. Androsch, M. L. Di Lorenzo, *Macromolecules* **2013**, *46*, 6048.
[42] R. Androsch, M. L. Di Lorenzo, Polymer **2013**, *54*, 6882.
[43] R. Androsch, M. L. Di Lorenzo, C. Schick, *Eur. Polym. J.* **2016**, *75*, 474.
[44] R. Androsch, M. L. Di Lorenzo, C. Schick, *Eur. Polym. J.* **2017**, *96*, 361.
[45] R. A.Andrianov, R. Androsch, R. Zhang, T. A. Mukhametzyanov, A. S. Abyzov, J. W. P. Schmelzer, C. Schick, *Polymer* **2020**, *196*, 122453.
[46] Luminy® PLA neat resins: PLA bioplastics for a brighter future. https://totalcorbion.4net-acc.com/media/iufhvey2/factsheet_luminy-pla-neat-resins_20190903.pdf (accessed Nov 3, 2021).
[47] G. Tammann, *Z. Phys. Chem.* **1898**, *25*, 441.
[48] G. Tammann, E. Jenckel, *Zeitschrift Für Anorg. Und Allg. Chemie.* **1930**, *193*, 76.
[49] D. Tammaro, V. Contaldi, M. G. P. Carbone, E. Di Maio, S. Iannace, *J. Cell. Plast.* **2016**, *52*, 533.
[50] K. Yu, J. Ni, H. Zhou, X. Wang, J. Mi, *Polymer* **2020**, *200*, 122539.
[51] M. C. Righetti, M. Gazzano, M. L. Di Lorenzo, R. Androsch, *Eur. Polym. J.* **2015**, *70*, 215.
[52] B. Li, G. Zhao, G. Wang, L. Zhang, J. Hou, J. Gong, *Int. J. Biol. Macromol.* **2019**, *129*, 171.
[53] B. Li, G. Zhao, G. Wang, L. Zhang, J. Gong, *Polym. Degrad. Stab.* **2018**, *156*, 75.
[54] L.Q. Xu, H.X. Huang, *Ind. Eng. Chem. Res.* **2014**, *53*, 2277.
[55] H. Marubayashi, S. Akaishi, S. Akasaka, S. Asai, M. Sumita, *Macromolecules* **2008**, *41*, 9192.
[56] M. Nofar, A. Tabatabaei, A. Ameli, C. B. Park, *AIP Conf. Proc.* **2014**, *1593*, 320.
[57] M. Nofar, W. Zhu, C. B. Park, *Polymer* **2012**, *53*, 3341.
[58] M. Dobrzyńska-Mizera, M. Knitter, A. Woźniak-Braszak, M. Baranowski, T. Sterzyński, M. L. Di Lorenzo, *Materials* 2020, *13*, 3776.
[59] M. Cocca, M. L. Di Lorenzo, M. Malinconico, V. Frezza, *Eur. Polym. J.* **2011**, *47*, 1073.
[60] S. J. J. Sheng, X. Hu, F. Wang, Q. Y. Y. Ma, M. F. F. Gu, *Mater. Sci. Eng. C.* **2015**, *49*, 612.
[61] J. Li, X. Liao, Q. Yang, G. Li, *Ind. Eng. Chem. Res.* **2017**, *56*, 11111.